ISSN 0021-3640, JETP Letters, 2018, Vol. 108, No. 5, pp. 318–325. © Pleiades Publishing, Inc., 2018.
Original Russian Text © P.V. Medvedev, M.A. Soldatov, V.V. Shapovalov, A.A. Tereshchenko, I.E. Gorban', A.G. Fedorenko, A.V. Soldatov, 2018, published in Pis'ma v Zhurnal Eksperimental'noi i Teoreticheskoi Fiziki, 2018, Vol. 108, No. 5, pp. 339–347.

CONDENSED MATTER

Analysis of the Local Atomic Structure of the MIL-88a Metal–Organic Framework by Computer Simulation Using XANES Data

P. V. Medvedev[a], *, M. A. Soldatov[a], V. V. Shapovalov[a], A. A. Tereshchenko[a], I. E. Gorban'[a], A. G. Fedorenko[a], and A. V. Soldatov[a]

[a] *International Research Center Smart Materials, Southern Federal University, Rostov-on-Don, 344090 Russia*

**e-mail: pavelmedvedev1994@gmail.com*

Received June 18, 2018; in final form, July 16, 2018

Experimental X-ray absorption spectra near the Fe *K* edge for as-synthesized MIL-88a metal–organic framework (MIL stands for Materials Institute Lavoisier) before and after activation have been obtained and analyzed for the first time. The theoretical analysis of experimental spectra has revealed changes in the local atomic structure of iron at the desorption of water from pores of the studied material in the process of activation.

DOI: 10.1134/S0021364018170083

1. INTRODUCTION

Metal–organic frameworks (MOFs) are widely studied now [1–3]. These compounds are crystal materials consisting of inorganic (clusters containing metal cations) and organic parts, linkers (carboxylates, phosphonates, imidazolates, etc.) [1, 4]. In addition to a crystal structure, MOFs have a developed porous structure [5]. An almost unlimited variety of combinations of organic and inorganic parts for synthesis makes it possible to obtain given physical and chemical properties of new materials in a wide range. In particular, MOFs can be synthesized with a flexible framework whose flexibility is manifested primarily in the processes of solvation and desolvation. Since crystallites obtained by solvothermal synthesis have a solvated form containing solvent molecules and reaction products, desolvation or, in other words, activation should be performed for their application in practice. The release of solvent molecules from pores of a flexible MOF at a high temperature and/or a low pressure changes the crystal lattice parameters, mutual orientation of molecules, volume of pores, and material surface area. This process is reversible and does not destroy the material, which allows multiple solvation/desolvation cycles. Because of this property, MOFs with a flexible frame are called "breathing" materials [6, 7].

Metal–organic frameworks also include a specific subclass of materials having a very low toxicity because of their chemical composition. Because of this property and the developed porous structure, they can be used as carriers for targeted drug delivery [8–12]. One of such materials is MIL-88a (MIL stands for Materials Institute Lavoisier), which was synthesized through the interaction of trivalent iron salts with fumaric acid. The compound of trivalent iron ions with fumarate ions forms a hexagonal system (P_{-62c}) with the chemical formula $Fe_3^{III}O(H_2O)_3\{-O_2C-C_2H_2-CO_2-\}_3 \cdot 19H_2O$ [7] (Fig. 1). The first coordination sphere of iron atoms in MIL-88a includes six oxygen atoms forming an octahedron [6, 7] (Fig. 1). The atom $O_{\mu 3}$ is common for three iron atoms, four equatorial atoms O_{c1}–O_{c4} belong to carboxyl groups of fumaric acid, and the atom O_w belongs either to a water molecule or to the hydroxyl group of methanol depending on the solvent used. The second coordination sphere includes atoms of fumaric acid and oxygen atoms of water molecules in pores.

In addition to biomedical applications, MIL-88a can also be used to obtain coals doped with γ-Fe_2O_3 nanoparticles for chemoselective hydration of nitrocompounds [13], to obtain Fe_3O_4 particles with a hierarchic structure for the creation of supercapacitors [14, 15], to obtain hollow MIL-88a microspheres [16], to stabilize biomacromolecules [17], and as a heterogeneous catalyst for photocatalytic oxidation reactions [18–20].

However, although potential applications of this MOF were discussed in numerous works [8–20], activation-induced changes in the local environment of iron have not yet been studied in detail. The process of activation is a necessary stage before impregnation of MOFs with bioactive molecules and directly affects

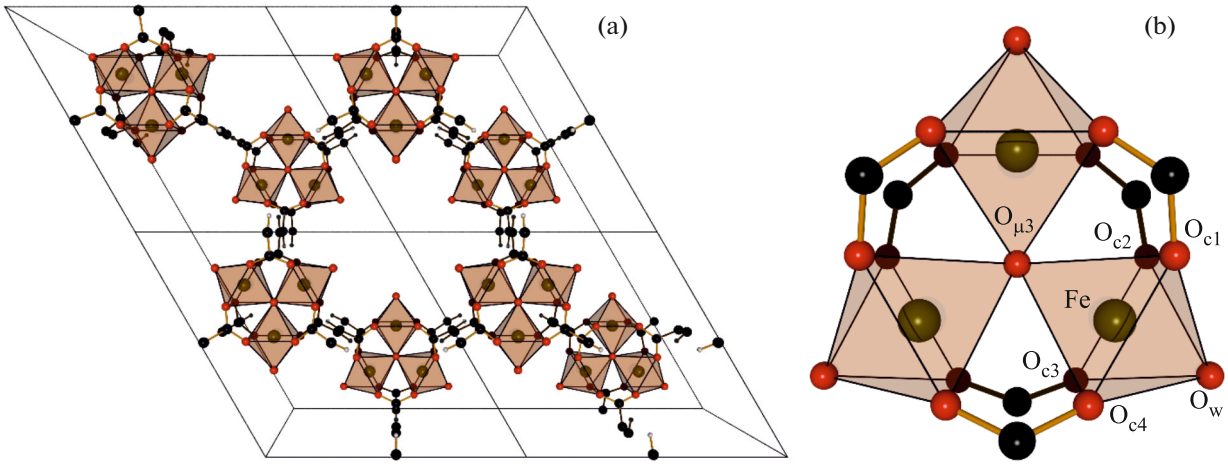

Fig. 1. (Color online) (a) MIL-88a $2 \times 2 \times 1$ supercell. (b) Iron trimer with specified oxygen atoms.

the efficiency of subsequent attachment of guest molecules. For this reason, it is important to reveal a mechanism of release of guest molecules at the activation of the MIL-88a MOF, as well as to determine changes in the local structure near iron atoms. These problems are solved using experimental and theoretical X-ray absorption near edge structure (XANES) methods. These methods are element selective and, in contrast to traditionally used X-ray diffraction, have a high sensitivity to change in the local atomic and electron structures around an absorbing atom even in materials without long-range order in atomic arrangement, which is very important for nanostructured materials [21, 22].

2. MATERIALS AND METHODS

Using previously described methods [4, 23], we performed hydrothermal synthesis of MIL-88a. To increase the mass of the synthesized sample, the synthesis parameters were modified by increasing the volume and concentration of the reaction mixture. Iron(III) chloride hexahydrate [$FeCl_3 \cdot 6H_2O$ 0.7781 g, 2.8 mmol, purity ≥98%, Sigma-Aldrich] was dissolved in deionized water (30 mL, Milli-Q, resistivity 18.2 MΩ cm at 25°C). After that, fumaric acid ($HO_2CCH{=}CHCO_2H$ 0.3248 g, 2.8 mmol, purity 99%, Alpha Aesar) was added to the solution. The resulting solution was placed in a 45-mL Teflon autoclave [Acid Digestion Vessel 4744, Parr Instrument Company] and was heated to 125°C using a magnetic stirrer with heating (stirring rate of 200 rpm). After 24 h, synthesized microcrystals were separated in a centrifuge from reaction by-products, unreacted materials, and water (10000 rpm, 7260 g, 10 min, Sigma 3-30KHS). Then, synthesized microcrystals were washed with deionized water and were dried at a temperature of 60°C.

Infrared spectra were recorded in the range of 500–3750 cm^{-1} using an FSM-1202 infrared Fourier transform spectrometer (Infraspek, Russia) by the transmission method with a resolution of 2 cm^{-1}. To this end, a synthesized sample was mixed with a dry potassium bromide powder in a mass ratio of 1 : 100; after that, this mixture was pressed into a 1-mm-thick pellet 200 mg in mass. To subtract the background, we used a pure potassium bromide pellet with the same parameters.

Diffraction patterns were recorded on a D2 Phaser X-ray diffractometer (Bruker, Germany) with Cu $K\alpha$ radiation ($\lambda = 1.54$ Å). The measurements were performed in a low-background cuvette with a resolution of 0.05° per step in the range of $2\theta = 5°–20°$ with an exposure time of 0.2 s per step.

Thermogravimetric curves were obtained on an STA 449 F5 Jupiter instrument (Netzsch, Germany) at the heating of the sample up to 200°C at a rate of 5°C per minute. Activation was performed in a corundum crucible at constant blowing by a dry mixture of nitrogen and oxygen (in a volume ratio of 78 : 22).

To determine the shape and size of synthesized crystallites, we obtained images on a Tecnai G2 BioTwin transmission electron microscope (FEI Company, United States) with an accelerating voltage of 120 kV.

To detect changes in the local atomic structure of an iron atom at the desorption of water molecules from MOFs, XANES spectra of as-synthesized and activated MIL-88a samples were measured in the energy range of 7050–7200 eV behind the Fe K edge. XANES spectra were recorded on an R-XAS Looper X-ray absorption spectrometer (Rigaku, Japan) in the "transmission" mode using a Ge (311) monochromator crystal ($\Delta E \approx 1.4$ eV). The incident radiation intensity was detected by an ionization chamber (Ar, 300 mbar), and the transmitted radiation intensity was

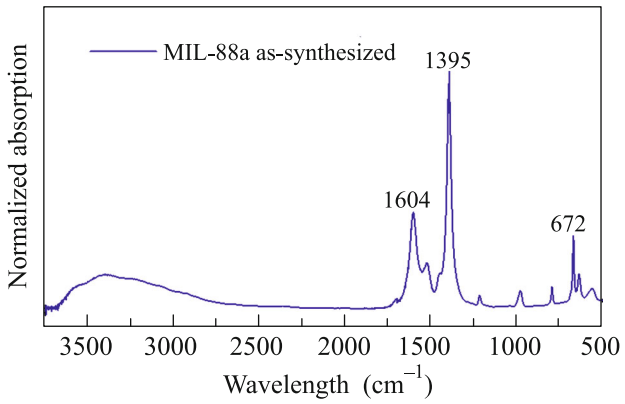

Fig. 2. (Color online) Infrared spectrum of the as-synthesized MIL-88a sample.

measured by an SC-70 scintillation detector. The samples were mixed with boron nitride and were pressed into a 1-mm-thick pellet, which was then activated. The optimal mass of the pellet sample 13 mm in diameter was calculated using the XAFSmass program [24]. Activation was performed at 150°C in a quartz cell equipped with built-in Kapton windows transparent in the X-ray range. This cell allows activation and X-ray diffraction measurements of the samples under controllable conditions of the environment (temperature and pressure) [25]. The cell with a sample was connected through an external vacuum line to a backing pump to remove physically adsorbed water (a resulting pressure of 10^{-6} bar). The activation time was 1 h without the heating time. After activation, the cell with the sample was cooled down to room temperature and hermetically sealed. Further, the sample was located in the cell at a low pressure during the measurements of XANES spectra.

Theoretical XANES spectra of the MIL-88a samples were calculated using an accelerated version of the FDMNES program [26]. The calculation method is based on the solution of the Schrödinger equation using the finite difference method on a three-dimensional mesh with a step of 0.2 Å and a radius of 7 Å. This approach is sensitive not only to structural changes directly around the iron atom but also to the orientation of the linker with respect to iron trimers. The R factor was calculated by the formula

$$R_f = \frac{\Sigma((I_{\text{exp}} - I_{\text{theor}})^2)}{\Sigma(I_{\text{exp}})^2}, \quad (1)$$

where R_f is the R factor of the theoretical spectrum and I_{exp} and I_{theor} are the experimental and theoretical spectral intensities in the energy range $(E; E + \partial E)$, respectively.

XANES spectra were normalized using the Demeter program [27].

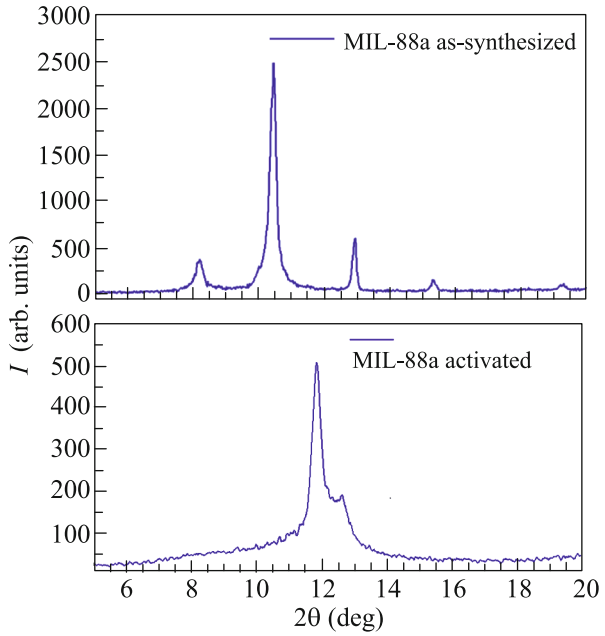

Fig. 3. (Color online) Diffraction patterns of the MIL-88a sample (a) after synthesis and purification and (b) after activation.

3. RESULTS AND DISCUSSION

A set of peaks on infrared spectra and diffraction patterns that is characteristic of this MIL-88a sample was identified in previous works [14, 18, 19]. The vibrational spectrum shown in Fig. 2 includes peaks of fumaric acid, which belong to asymmetric (1605 cm^{-1}) and symmetric (1395 cm^{-1}) vibrations of the carboxyl group, as well as to vibrations of carbonyl group (672 cm^{-1}). In addition to these peaks, the spectrum contains a wide range (3600–2800 cm^{-1}), which is due to vibration of water adsorbed by the framework.

The most intense reflections on the diffraction pattern of the MIL-88a sample at 8°–9°, 10°–11°, and 12°–13° (Fig. 3) come from the (100), (101), and (002) reflection planes, respectively. The positions of peaks on the diffraction pattern for different samples immediately after synthesis can be slightly different in view of a very high flexibility of the framework [6, 7] and different amounts of water stored in its pores, However, after activation in a backing vacuum of 3×10^{-6} bar, the samples obtained in different synthesis processes but under identical conditions acquire the same structure—activated MIL-88a form (Fig. 3).

Transmission electron microscopy (TEM) images (Fig. 4) demonstrate that the as-synthesized sample consists primarily of elongated microcrystals with a mean length of 4.5 μm and a mean width of 1.2 μm (Fig. 5).

In the process of heating of the sample, which is accompanied by the release of water from the framework, the sample is noticeably darkened, changing its

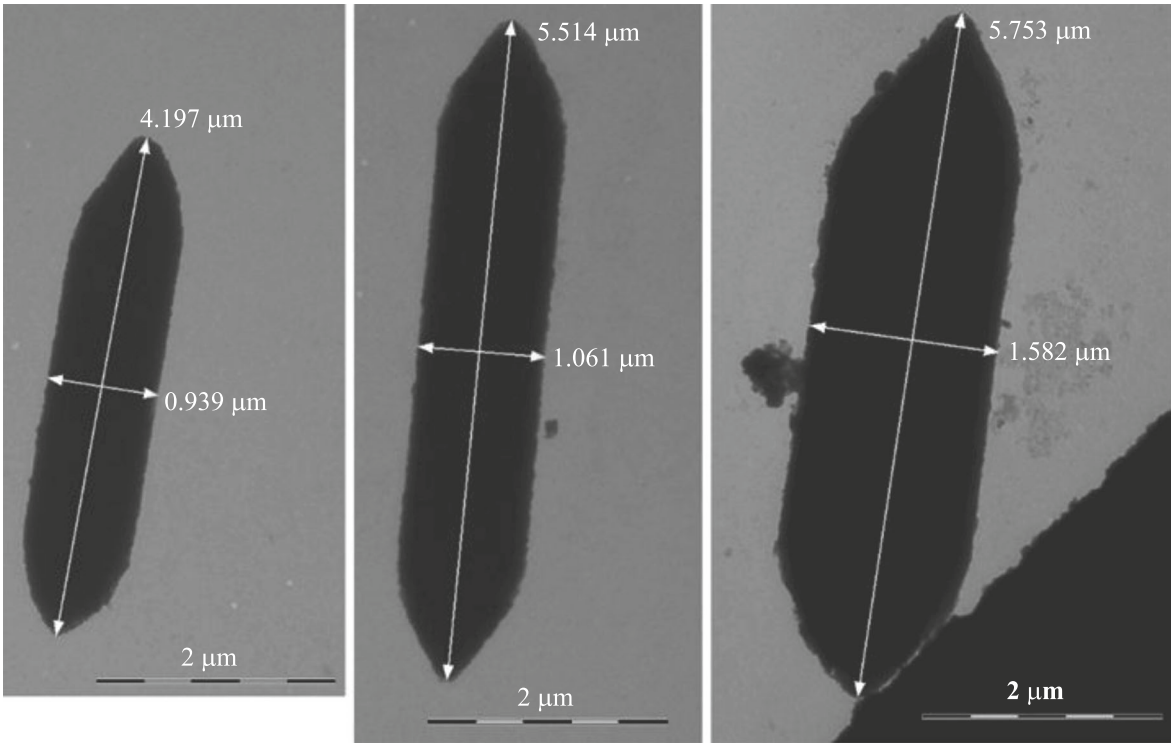

Fig. 4. TEM images of the as-synthesized sample.

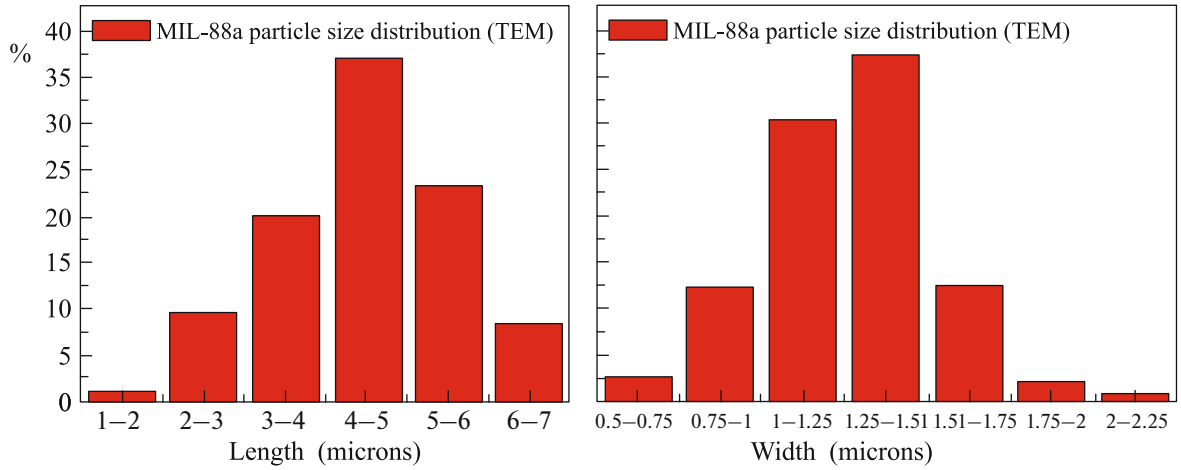

Fig. 5. (Color online) Particle size distribution in the MIL-88a sample according to the TEM data.

color from light orange to brown. Such a change in color can be explained by change in the local environment of iron in the process of desorption of water from the framework. In the previously determined structures of the open and activated forms of the framework of the MIL-88a sample [6], it was found that complete activation leads to the deformation of the framework accompanied by a change in the unit cell parameters and the mutual arrangement of atoms. However, the change in color can also be due to the detachment of the oxygen atom O_w, which can belong to a water or methanol molecule [23] and form a bond immediately with the iron atom.

In previous work [7], the chemical formula of MIL-88a was determined as $(Fe_3^{III}O(H_2O)_3\{-O_2C-C_2H_2-CO_2-\}_3 \cdot 19H_2O)$. According to this formula, water molecules in the first coordination sphere of iron constitute 5.5 wt %, whereas other water molecules in pores amount to 34.5 wt %. According to the gravimetric analysis (Fig. 6), the sample at heating to

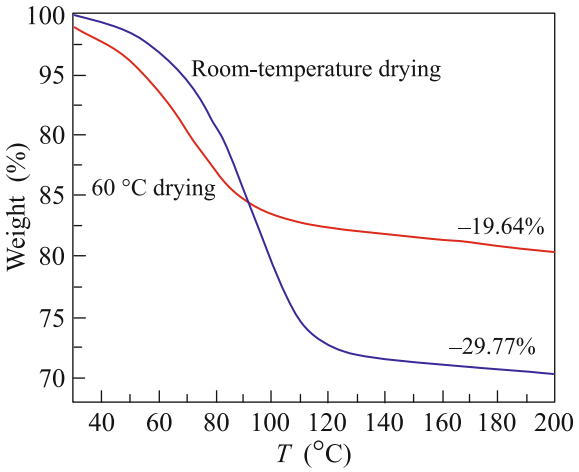

Fig. 6. (Color online) Thermogravimetric curve of the MIL-88a sample after synthesis and purification.

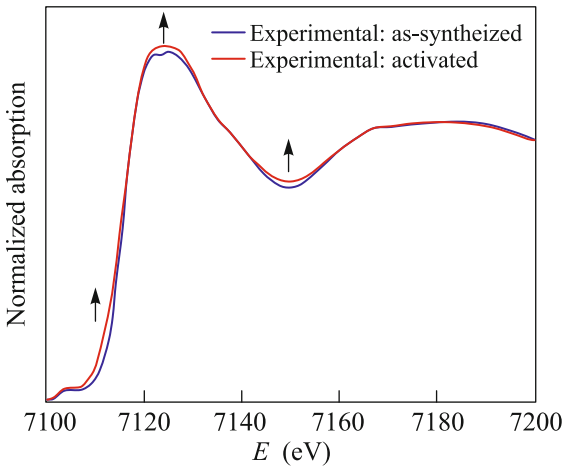

Fig. 7. (Color online) Normalized XANES spectra of MIL-88a samples before and after activation.

200°C loses 29.77 wt %, primarily at 110–120°C, above which the sample hardly loses mass. The thermogravimetric curve of the sample dried after washing at a temperature above room temperature, e.g., at 60°C (Fig. 6) will demonstrate a smaller loss of mass.

However, although activation is accompanied by a noticeable loss of weight and by changes in the structure, no noticeable changes in XANES spectra before and after activation were observed (Fig. 7). This activation does not lead to the shift of the absorption edge and a change in its shape, which indicates that the geometry of the iron environment, as well as the degree of oxidation, does not change at the desorption of water.

To analyze the results obtained, we calculated theoretical XANES spectra within various structural models of MIL-88a, which are based on previous works [6, 7]. The first pair of models describe the framework of MIL-88a immediately after synthesis and purification (Fig. 8). Pores in the material are maximally expanded and contain oxygen atoms belonging to water molecules in pores of the framework. The crystal lattice parameters in both models of an open structure are the same ($a = 13.871$ Å, $b = 13.871$ Å, $c = 12.663$ Å). The first model of the open structure (model I) is the framework where oxygen atoms form regular octahedra around iron atoms. The distances from oxygen atoms to iron are approximately identical (Table 1). In the second model of the open structure (model II), octahedra are deformed and the distances from the vertices of octahedra to the central iron atoms are significantly different.

The second pair of models corresponds to activated MIL-88a, where all guest molecules leave the pores of the framework in the process of activation under the effect of temperature and vacuum, which leads to the closure of pores. Model III includes the same set of atoms as model I and has an almost identical set of trimers, but differs primarily in crystal lattice parameters ($a = 9.7798$ Å, $b = 9.7798$ Å, $c = 14.8265$ Å) and in orientation of fumaric acid molecules relative to iron trimers. Model IV corresponding to the MIL-88a structure with closed pores includes the same set of atoms as model III and has the same crystal lattice parameters, but differs in the absence of the oxygen atom O_w in the first coordination sphere. This model is used to test the assumption that the process of activation can lead to the breaking of the Fe–O_w bond with the subsequent escape of a water molecule from the first coordination sphere of iron.

Since the profile of the XANES spectrum is sensitive to the distance to the nearest atoms, bond angles, and atomic number, the real positions of atoms can be found with a high accuracy of 0.02 Å by analyzing theoretical models [28].

The comparison of the spectra shows that the regular octahedral environment forms the absorption edge profile similar to a parabola, whereas the

Table 1. Distances from iron atoms to atoms of the first coordination sphere

Bond	Bond length, Å			
	Model I	Model II	Model III	Model IV
Fe–$O_{\mu 3}$	1.94	1.84	2.01	2.01
Fe–O_w	1.94	1.95	1.91	–
Fe–O_{C1}	1.91	2.13	1.83	1.83
Fe–O_{C2}	1.91	2.21	1.87	1.87
Fe–O_{C3}	1.91	2.13	1.83	1.83
Fe–O_{C4}	1.91	2.21	1.87	1.87

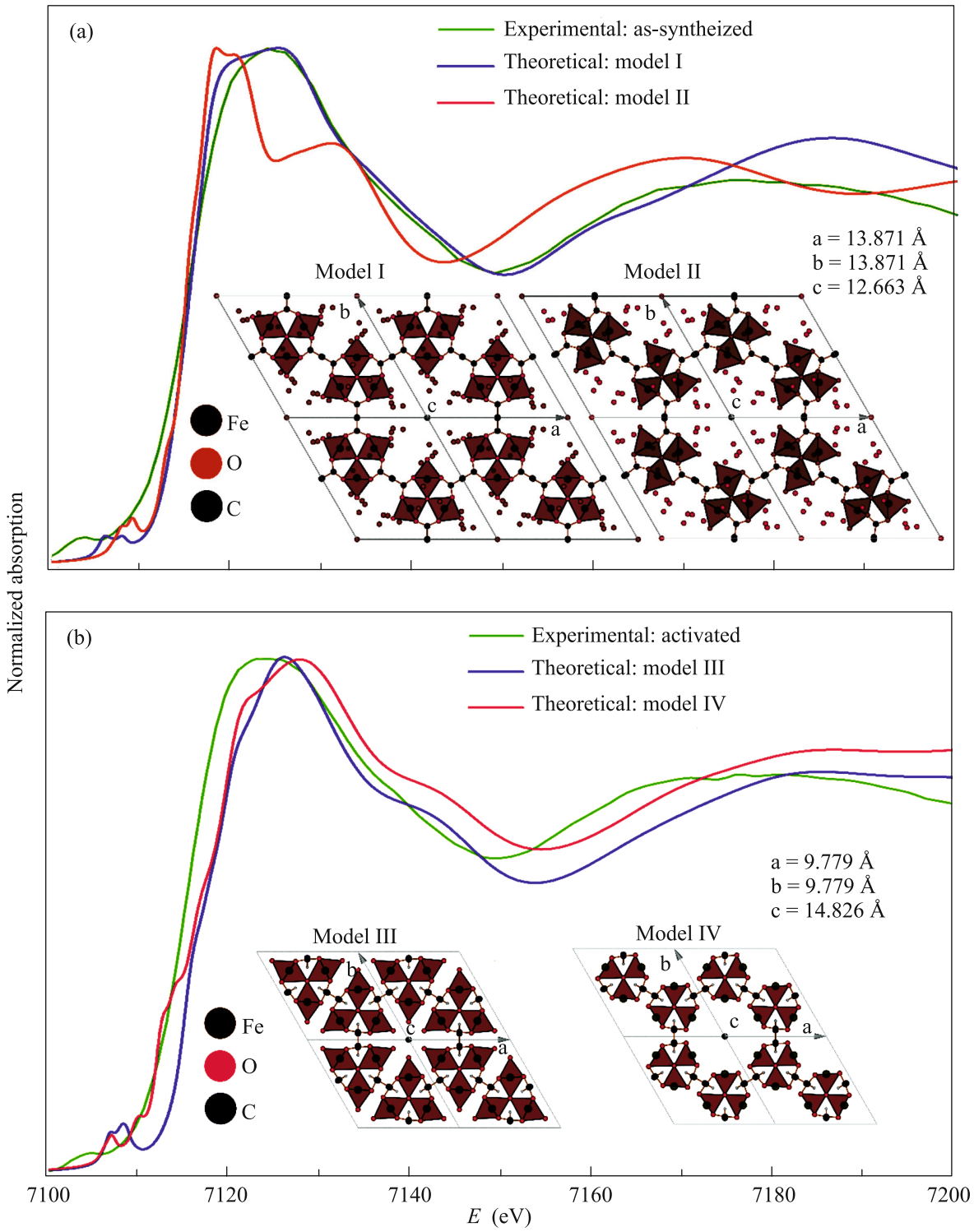

Fig. 8. (Color online) (a) XANES spectrum measured for the as-synthesized MIL-88a sample in comparison with theoretical spectra calculated for structural models with open pores (models I and II). The inset shows structural models for a phase with open pores. (b) XANES spectrum measured for the activated MIL-88a sample in comparison with theoretical spectra calculated for structural models with closed pores (models III and IV). The inset shows structural models for a phase with closed pores.

deformed octahedron separates the absorption edge into two features—the most intense absorption in the range of 7115–7125 eV and a "shoulder" in the range of 7125–7140 eV. As a result, the absorption edge shape in the spectrum calculated within structural model I is in good agreement with the experimental

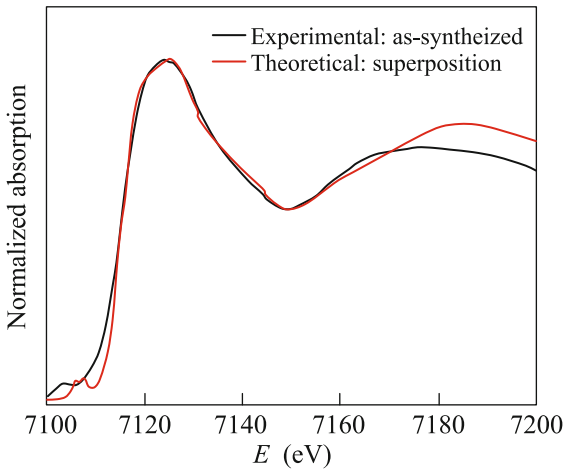

Fig. 9. (Color online) Experimental spectrum of the MIL-88a sample in comparison with the superposition of theoretical spectra for models I and III.

spectrum (cf. $R_f^{\text{Model I}} = 0.033$ and $R_f^{\text{Model II}} = 0.510$), but has some differences. This can mean that a part of the sample used to measure the experimental spectrum before activation can have some structural defects or can contain other phases of the MIL-88a structure.

Since partial activation of the samples can occur at a temperature of sample drying of 60°C [19], it was assumed that an additional phase is the activated form of MIL-88a, which corresponds to model III.

The comparison of the spectra indicates that the experimental spectral profile before activation can be reproduced by the superposition of theoretical spectra calculated within structural models of hydrated (model I) and activated (model III) forms.

This superposition can provide the spectrum of a material including 74 vol % of the open form of MIL-88a and 26 vol % of activated MIL-88a (Fig. 9). The R factor of the spectrum of such a combination is one quarter of that for the spectrum of the open structure ($R_f^{\text{SP}} = 0.0088$ for the mixed spectrum versus $R_f^{\text{Model I}} = 0.0335$), which indicates better agreement with the experiment. Such a material should be crystallites with the core–shell structure, where the core and shell contain the hydrated and activated forms of MIL-88a, respectively. Thus, being a structure with compressed pores, this shell prevents the desorption of water molecules from the inner volume.

4. CONCLUSIONS

Experimental XANES spectra have been obtained for the first time for a hydrothermally synthesized MIL-88a metal–organic framework polymer sample before and after activation. The comparison of experimental XANES spectra with theoretical spectra for structural models has indicated that the sample purified after hydrothermal synthesis and dried at 60°C consists of crystals with a core–shell structure. The core constituting 74 vol % of the entire sample contains the hydrated form of MIL-88a, whereas the shell has the activated form. The activation of such a material at 150°C for 1 h at a reduced pressure leads only to insignificant changes in the absorption edge intensity because the shell prevents the evaporation of water from the core of crystallites. In this process, no chemical shift occurs and the edge shape does not change, which indicates that the local environment and degree of oxidation of iron do not change at activation.

This work was performed within research assignment no. VnGr-07/2017-08, Southern Federal University project “X-ray Diffraction Study with Research Megafacilities (Including *Operando* Mode) and Multiscale Supercomputer Simulation of the Parameters of the Electronic Structure of Promising Materials Including Nanocomposites.” The work of M.A.S. was supported by the Council of the President of the Russian Federation for State Support of Young Scientists and Leading Scientific Schools (project no. SP-377.2016.4).

REFERENCES

1. G. Ferey, Chem. Soc. Rev. **37**, 191 (2008).
2. V. V. Butova, M. A. Soldatov, A. A. Guda, K. A. Lomachenko, and C. Lamberti, Russ. Chem. Rev. **85**, 280 (2016).
3. L. Sarkisov, R. L. Martin, M. Haranczyk, and B. Smit, J. Am. Chem. Soc. **136**, 2228 (2014).
4. T. Chalati, P. Horcajada, R. Gref, P. Couvreur, and C. Serre, J. Mater. Chem. **21**, 2220 (2011).
5. C. V. McGuire and R. S. Forgan, Chem. Commun. **51**, 5199 (2015).
6. C. Serre, C. Mellot-Draznieks, S. Surble, N. Audebrand, Y. Filinchuk, and G. Ferey, Science (Washington, DC, U. S.) **315**, 1828 (2007).
7. C. Mellot-Draznieks, C. Serre, S. Surble, N. Audebrand, and G. Ferey, J. Am. Chem. Soc. **127**, 16273 (2005).
8. C. Tamames-Tabar, D. Cunha, E. Imbuluzqueta, F. Ragon, C. Serre, M. J. Blanco-Prieto, and P. Horcajada, J. Mater. Chem. B **2**, 262 (2014).
9. P. Horcajada, R. Gref, T. Baati, P. K. Allan, G. Maurin, P. Couvreur, G. Ferey, R. E. Morris, and C. Serre, Chem. Rev. **112**, 1232 (2012).
10. A. C. McKinlay, J. F. Eubank, S. Wuttke, B. Xiao, P. S. Wheadey, P. Bazin, J. C. Lavalley, M. Daturi, A. Vimont, G. de Weireld, P. Horcajada, C. Serre, and R. E. Morris, Chem. Mater. **25**, 1592 (2013).
11. P. Horcajada, T. Chalati, C. Serre, B. Gillet, C. Sebrie, T. Baati, J. F. Eubank, D. Heurtaux, P. Clayette, C. Kreuz, J. S. Chang, Y. K. Hwang, V. Marsaud, P. N. Bories, L. Cynober, S. Gil, G. Ferey, P. Couvreur, and R. Gref, Nat. Mater. **9**, 172 (2010).

12. D. Cunha, M. Ben Yahia, S. Hall, S. R. Miller, H. Chevreau, E. Elkaim, G. Maurin, P. Horcajada, and C. Serre, Chem. Mater. **25**, 2767 (2013).
13. Y. Li, Y. X. Zhou, X. Ma, and H. L. Jiang, Chem. Commun. **52**, 4199 (2016).
14. L. Wang, Y. Y. Zhang, X. Li, Y. Z. Xie, J. He, J. Yu, and Y. H. Song, Sci. Rep. **5**, 14341 (2015).
15. L. Wang, J. Yu, X. T. Dong, X. Li, Y. Z. Xie, S. H. Chen, P. Li, H. Q. Hou, and Y. H. Song, ACS Sustain. Chem. Eng. **4**, 1531 (2016).
16. G. Y. Jeong, R. Ricco, K. Liang, J. Ludwig, J. O. Kim, P. Falcaro, and D. P. Kim, Chem. Mater. **27**, 7903 (2015).
17. K. Liang, R. Ricco, C. M. Doherty, M. J. Styles, S. Bell, N. Kirby, S. Mudie, D. Haylock, A. J. Hill, C. J. Doonan, and P. Falcaro, Nat. Commun. **6**, 8 (2015).
18. K. Y. A. Lin and S. Y. Chen, RSC Adv. **5**, 43885 (2015).
19. K. Y. A. Lin, H. A. Chang, and C. J. Hsu, RSC Adv. **5**, 32520 (2015).
20. W. T. Xu, L. Ma, F. Ke, F. M. Peng, G. S. Xu, Y. H. Shen, J. F. Zhu, L. G. Qiu, and Y. P. Yuan, Dalton Trans. **43**, 3792 (2014).
21. G. Smolentsev and A. Soldatov, J. Synchrotr. Radiat. **13**, 19 (2006).
22. A. V. Soldatov, Soros. Obrazov. Zh. **12**, 101 (1998).
23. C. Serre, F. Millange, S. Surble, and G. Ferey, Angew. Chem. Int. Ed. **43**, 6286 (2004).
24. www.cells.es/Beamlines/CLAESS/software/xafsmass.html.
25. http://www1.fips.ru/fips_servl/fips_servlet?DB=RUPM&DocNumber=173869&TypeFile=html.
26. S. A. Guda, A. A. Guda, M. A. Soldatov, K. A. Lomachenko, A. L. Bugaev, C. Lamberti, W. Gawelda, C. Bressler, G. Smolentsev, A. V. Soldatov, and Y. Joly, J. Chem. Theory Comput. **11**, 4512 (2015).
27. B. Ravel and M. Newville, J. Synchrotr. Radiat. **12**, 537 (2005).
28. G. Yu. Smolentsev, Cand. Sci. (Phys. Math.) Dissertation (Rostov-on-Don, 2006).

Translated by R. Tyapaev